Eur. Phys. J. B **11**, 455–462 (1999)

THE EUROPEAN PHYSICAL JOURNAL B

EDP Sciences

Synchrotron X-ray study of the q-fold quasicrystalline symmetry of the Smectic C Twist Grain Boundary phase (TGB_C)

P. Barois[1], F. Heidelbach[2], L. Navailles[3,a], H.T. Nguyen[1], M. Nobili[1,3], M. Petit[1], R. Pindak[4], and C. Riekel[2]

[1] Centre de Recherche Paul Pascal, CNRS, avenue A. Schweitzer, 33600 Pessac, France
[2] E.S.R.F, B.P. 220, 38043 Grenoble, France
[3] G.D.P.C.[b], Université Montpellier II, 34000 Montpellier, France
[4] Bell Labs, Lucent Technologies, Murray Hill, NJ 07974, USA

Received 18 January 1999

Abstract. We report the first X-ray scattering investigation of spatial variations of the q-fold quasicrystalline symmetry (so-called commensurability) of well-aligned TGB_C samples. A spatial resolution of 20×40 μm^2 was achieved using the ESRF microfocus beamline. The liquid crystal samples, contained between glass plates which were either parallel or in a wedge geometry, were scanned in order (i) to probe the mosaicity and (ii) to continuously change the balance between surface and volume effects. In the case of parallel plate cells, commensurability was observed everywhere throughout the sample, hence ruling out possible effects of mosaicity to explain the q-fold symmetry of the diffraction patterns previously reported when probed with a spatial resolution of 1×1 mm^2 in rotating anode experiments. In the case of wedge cells, the evolution of X-ray patterns with thickness suggested that commensurate lockin occurs for sufficiently thick samples with a width that is statistical.

PACS. 61.30.Eb Experimental determinations of smectic, nematic, cholesteric, and other structures – 61.10.-i X-ray diffraction and scattering

1 Introduction

The analogy between the nematic (N) to smectic A (SmA) transition in liquid crystals and the normal to superconductor transition in metals was first recognised by de Gennes in 1972 [1]. According to the analogy, the application of a chiral field to a SmA liquid crystal is analogous to the application of a magnetic field to a superconductor.

On the theoretical front, Renn and Lubensky (RL) [2] predicted a specific model for the liquid crystal analog of the Abrikosov flux phase appearing in type II superconductors. The new highly dislocated smectic A phase expected in chiral systems was called the Twist Grain Boundary SmA (TGB_A for short). Its structure consists of SmA slabs of constant thickness l_b stacked in a helical fashion along an axis x parallel to the smectic layers of thickness d. Adjacent slabs are connected by a twist grain boundary made of parallel screw dislocation of average separation l_d. The rotation angle Δ of the smectic layers across a grain boundary satisfies $d = 2\, l_d \sin(\Delta/2)$. The existence of two additional TGB phases was predicted between the N^* and SmC^* phases: TGB_C and TGB_{C^*} phases [3]. The three TGB phases differ by the nature of the slabs, respectively smectic A, smectic C and smectic C^*.

Renn and Lubensky [2] showed that the nature of the TGB state depends on the value of the twist angle $\Delta = 2\pi\alpha$. If α is irrational, no periodicity exists along the pitch axis x and the state is incommensurate; if on the other hand α is rational (say $\alpha = p/q$ with p, q mutually prime integers), the structure is commensurate instead and x is a q-fold screw axis. If this screw axis is not crystallographically allowed (*i.e.* if $q \neq 2$, 3, 4 or 6), the TGB state has quasicrystalline rather than periodic crystalline symmetry and is incommensurate in the plane $y - z$ perpendicular to the pitch axis. As pointed out by Renn and Lubensky [2], X-ray scattering is intense on a Bragg cylinder of radius $Q_0 = 2\pi/d$ and finite height ξ^{-1} along x (reflecting the finite extension l_b of the smectic slabs along x) in the incommensurate state. For the commensurate TGB phase with non crystallographic q, the fundamental set of reciprocal vectors forms a ring (of radius Q_0) of equally spaced Bragg spots in the $Q_y - Q_z$ plane, perpendicular to the screw axis. Considering the exponentially small interaction between screw dislocations, the occurrence of a commensurate lockin of α on rational values was however expected to be unlikely.

On the experimental front, Goodby *et al.* [4] reported in 1989 the discovery of the first TGB phase on a chiral

[a] e-mail: navailles@crpp.u-bordeaux.fr
[b] UMR 5581 du CNRS

compound. Optical, calorimetric and X-ray investigations were all consistent with the RL model for an incommensurate TGB_A. The TGB_C phase was later discovered by Nguyen *et al.* [5] in a new series of tolane derivatives which reproduces remarkably well the theoretical phase diagram of Renn hence confirming the validity of the criterion for the existence of type II behavior (analogous to the Ginzburg criterion for superconductors). Interestingly, the TGB_C structure was found commensurate at all temperatures [6]: X-ray experiments performed with a rotating anode generator on a well aligned sample showed a q-fold modulation of the scattering in the plane $Q_y - Q_z$ with $q = 16$, 18, 19 or 20. It is worth noting that any commensurate lockin on rational fractions p/q with values of q higher than approximately 45 would not be resolved by the collimation used to achieve reasonable count-rates in a standard rotating anode X-ray spectrometer where the typical angular resolution around the ring of scattering is about 7-8 degrees. The 45-fold diffraction pattern would appear as a uniform ring and be considered incommensurate. No incommensurate patterns were found throughout the temperature range. Instead, first order transitions (with hysteresis) between states with different but low values of q (16 to 20) were observed. The ratios for the rational fraction p/q, which were most consistent with the data, were ratios with $p = 1$. Larger values for p would require higher-angle, more energetic grain boundaries. Moreover, larger p values would imply larger slab lengths, l_b, and hence sharper diffraction features along the helical axis than observed experimentally.

Subsequent experiments performed on TGB_C phases of various chiral series [7] confirmed the systematic observation of a q-fold symmetry with observed values of q ranging from 11 to 25. A natural conclusion could be that unlike TGB_A, the TGB_C structures are always commensurate. If so, these observations should stimulate theoretical work since the interaction responsible for the commensurate lockin is so far unknown. Unfortunately, the reported experiments do not constitute a proof of existence of an intrinsic commensurate lockin and the observations must be taken cautiously: experimental samples are always of limited thickness (25 μm in most experiments which corresponds to 8 to 80 helical pitches, depending on chemical series and temperature). One may then suspect that the observed q-fold modulation is a finite size artefact that would not survive for thicker samples. Galerne for instance [8] argued that any real TGB_C sample is commensurate by construction if one assumes that both the number n_b of smectic slabs and the number n of helical pitches across the sample are integer: the commensurability ratio $\alpha = p/q$ simply equals n/n_b. The systematic observation of only low values of q is explained by a systematic coexistence of regions with different values of n/n_b (due to experimental gradients in both thickness and temperature). Any X-ray beam wider than the typical size of such p/q-mosaicity would then pick up regions with different ratios p/q. The regions with integer lockins (*e.g.* $p/q = 1/18$, $1/19$, etc...) would dominate the diffraction patterns since they would contribute to discrete spots whereas the regions with higher order rational p/q (*e.g.* $p/q = 10/181 \approx 1/18$) would contribute only to the diffuse ring of scattering. Although this is a plausible scenario, the starting assumptions are questionable. First, the number of helical pitches across a real sample is usually not integer since the anchoring directions on the top and bottom plates are not exactly parallel. Furthermore, an integer number of slabs requires that all slabs have the same thickness, including the slabs at the surfaces, which is not guaranteed. Hence, the important question of the effects of surface anchoring, finite size samples and p/q-mosaicity remains.

A natural experimental answer to the finite size problem would be to perform X-ray scattering experiments on samples of increasing thickness. This is unfortunately not feasible since the quality of the alignment falls off quickly for thicknesses above 25 μm. Probing the p/q-mosaicity requires an intense X-ray beam of size much smaller than the usual 1×1 mm^2 which can be achieved, with reasonable count-rates, on a rotating anode spectrometer.

In this paper, we report the first X-ray experiment performed on well-aligned samples of the TGB_C phase, using a synchrotron line with a microfocus beam. The idea was (i) to probe the p/q-mosaicity of a well aligned TGB_C sample with a beam size smaller than the thickness and (ii) to change continuously the balance between surface and volume effects by changing the thickness. This was achieved by scanning a microfocus beam (20×40 μm^2) (i) across a cell of constant thickness and (ii) across a wedge cell. The p/q-mosaicity could then be probed within an area over 10^3 smaller than in the rotating anode experiment.

Experimental details are presented in Section 2. We will report successively the mesomorphic properties of the compound, the preparation of the sample, the optical check of the alignment and the X-ray beam line configuration. Finally, the results are described and discussed in Section 3.

2 Experimental details

The liquid crystal compound was the (S) enantiomer of the $n = 12$ homolog of the series of tolane derivatives having the general formula :

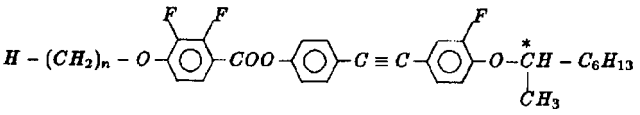

$n\mathrm{F_2BTFO_1M_7}$ for short.

Previous experiments [6] showed that the phase sequence (upon heating) is :

Crystal - 36.6 - SmC* - 102.6 - TGB_C - 103 - Cholesteric - 111.7 - Isotropic

The transition temperatures (in °C) were determined by differential scanning calorimetry (using a Perkin Elmer DSC 7). Most experiments were performed upon cooling for which the TGB_C temperature range is wider (from 102.8 to 101.7 °C). Helical pitch measurements were performed in thin wedges using the Cano wedge method [9].

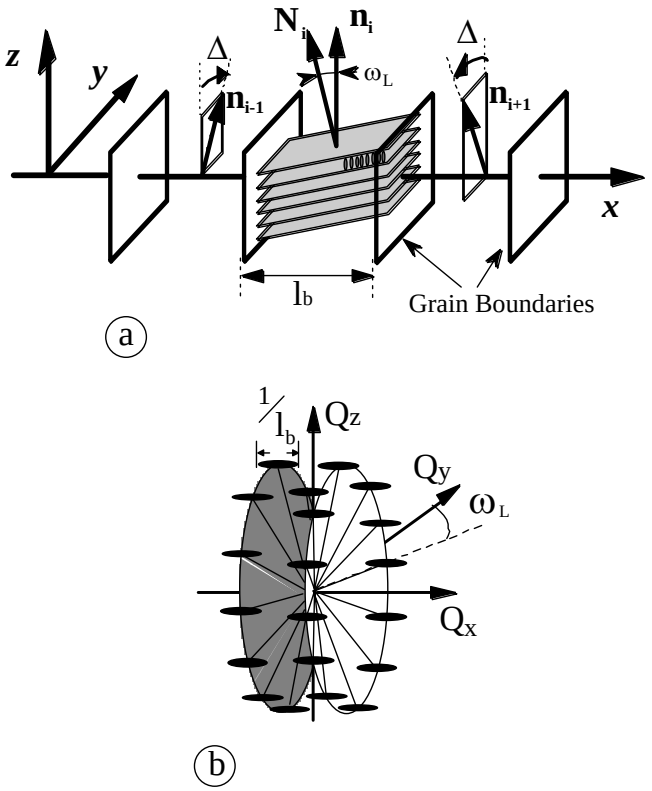

Fig. 1. Direct space (a) and reciprocal space (b) structure of the TGB_C phase. n_i and N_i are respectively the director field and the layer normal in slab $\#i$. For $12F_2BTFO_1M_7$, the tilt angle ω_L of the smectic layers is of order 13 degrees and the number of Bragg spots per ring varies from 16 to 22 with temperature.

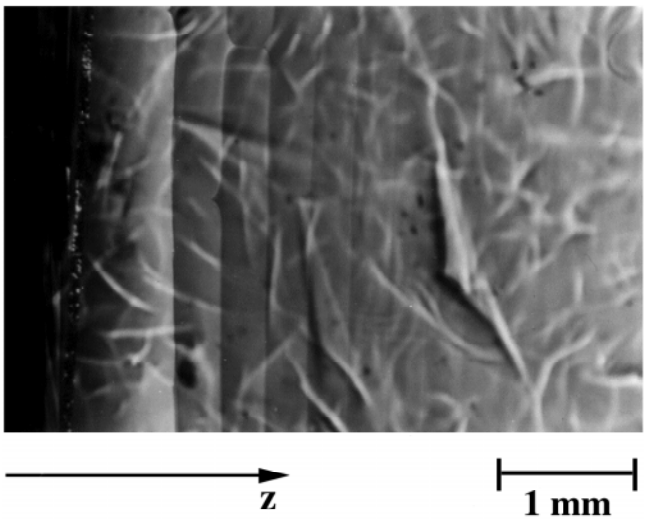

Fig. 2. Photograph of the TGB_C phase under polarizing microscope in a wedge of angle 0.4 degrees at $T = 102.2\,^{\circ}C$. The spacing of the Grandjean-Cano lines corresponds to a pitch of order 2 μm. Note that the rough dowstream plate (etched with hydrofluoric acid) introduce irregular textures on the photograph.

Upon cooling, the pitch increases strongly from 0.75 μm at the N^*-TGB_C transition to 3 μm at the TGB_C-SmC^* transition. X-ray experiments on well aligned samples have revealed the commensurability of the TGB_C phase but also showed [10] that it differs from the picture originally proposed by Renn and Lubensky [3]: the layers are tilted by an angle ω_L relative to the screw axis x. The director and the spontaneous polarisation of each slab are both essentially perpendicular to x. The structure of adjacent slabs follows from a rotation by an angle Δ across each grain boundary [10]. Figure 1 sketches the TGB_C structure in real and reciprocal space. No theoretical model has been developed so far to calculate the profile of the smectic order parameter $\Psi(x)$ across a smectic C slab of the TGB_C phase. However, like in TGB_A mesophases, the finite thickness of the slabs along x produces a finite extension of the Bragg spots along Q_x. The TGB_C reciprocal space is comprised of a set of two rings of Bragg rods parallel to Q_x.

Well aligned liquid crystal cells were prepared as discussed elsewhere [6] from two 150 μm thick glass plates. Planar boundary conditions were obtained by spin coating the inner surface of the glass plates with a polymer solution (polyvinylalcohol in water) which was then unidirectionally buffed with an appropriate velvet cloth. Absorption of X-rays by glass was reduced by etching the outer surface of the glass plates with hydrofluoric acid to a thickness of about 50 μm. Parallel cells were assembled with calibrated spacers (two 25 μm parallel gold wires 3 mm apart) whereas the wedge was formed by insertion of a 38 μm gold wire parallel to the edge at a distance of 6 mm. The resulting wedge angle was about 0.4°. For the wedge cell, only the downstream plate was etched in order to insure sufficient rigidity. All cells were filled by capillarity in the isotropic phase. The alignment was achieved by cooling into the cholesteric phase. The quality of the alignment was monitored by optical observation using a polarizing microscope. In wedge cells, a regular array of Grandjean-Cano (GC) steps formed rapidly. The samples were then cooled down to the TGB_C phase in which a Grandjean texture was preserved. Figure 2 shows the texture of the TGB_C phase at 102.2 °C. A regular array of GC steps parallel to the edge is observed (with a periodicity larger than in the cholesteric phase since the helical pitch is longer). The spacing of the very first GC step near the edge is often about twice the regular spacing. This could be due to curvature of the etched glass plate and/or a local structural change induced by the strong confinement conditions. Note that the rough downstream plate (etched with hydrofluoric acid) introduce irregular textures on the photograph.

X-ray scattering experiments were performed on the microfocus beamline (ID13) at the European Synchrotron Radiation Facility (E.S.R.F.). The X-ray beam was generated by an undulator in a low beta section of the ring. The beam was first monochromatized with a liquid N_2 cooled Si (111) channel cut monochromator and then focused with an ellipsoidal mirror. The final beam size was 20×40 μm^2 ($V \times H$) at sample position. With the selected energy of 13.0 keV, corresponding to a wavelength of 0.95 Å, the incident beam intensity was around 10^{11} photons/second. The X-ray scattering

patterns were recorded on an area detector located 1 m downstream from the sample. We used a sensitive CCD detector commercially available from Photonics Science. The X-ray scintillator screen was fiber-optically coupled to a CCD camera. The active detector area was $11.5(H) \times 8.6(V)$ cm^2 and the pixel resolution was 150 μm. The different divergences in the horizontal and vertical directions lead to the observation of Bragg spots elongated in the horizontal direction. The two stage oven was mounted on a *theta-Y-Z* stage and the temperature of the sample was controlled to a precision of ± 10 mK. The sample cell was mounted vertically (*i.e.* perpendicular to the beam) with the help of a laser collinear with the X-ray beam (defining the X-axis). The average helical axis of the TGB_C phase was then parallel to X. As shown in Figure 1b, the principal reciprocal lattice vectors of the TGB_C structure lie on two cones of axis Q_x and vertex angle $2\omega_L$. Unlike TGB_A, the whole set of fundamental reciprocal vectors cannot sit close to the Ewald's sphere. The theta angle was then rotated by $\omega_L = 12.5$ degrees to bring the center of one Bragg rod corresponding to a reciprocal vectors $\mathbf{Q}_1$ onto the Ewald's sphere close to the horizontal plane. Figure 3a shows the scattering geometry. The TGB_C reciprocal space intersects the Ewald's sphere at three points of maximum intensity: the chosen $\mathbf{Q}_1$, but also $\mathbf{Q}_2$ and $\mathbf{Q}_3$. Upon moving away from these three points, the Ewald's sphere still intersects the Bragg rods, but farther away from their center. The expected diffraction pattern (Fig. 3b) is a set of Bragg spots distributed on two arcs of a ring of radius $Q_0 = 2\pi/d \approx 0.168$ Å^{-1}. The intensity of the spots is maximum at positions $\mathbf{Q}_1$, $\mathbf{Q}_2$ and $\mathbf{Q}_3$ and falls off rapidly upon moving away from these three particular positions. Note that $\mathbf{Q}_2$ and $\mathbf{Q}_3$ rather than $-\mathbf{Q}_1$ fall on Ewald's sphere since $-\mathbf{Q}_1$ is off exact Bragg incidence by twice the Bragg angle $2\theta_B \approx 1.4$ degrees. The Ewald's sphere may intersect the TGB_C reciprocal space at most at the center of four Bragg rods instead of three with appropriate incidence (*e.g.* small clockwise rotation of the sample in Fig. 3a). In any case, the lack of inversion symmetry $\mathbf{Q} \leftrightarrow -\mathbf{Q}$ of the pattern reflects the curvature of the Ewald's sphere.

Let us note finally that the local smectic C order is one dimensional so that true long range order is in principle disrupted by thermal fluctuations. This well known effect, referred to as the Landau-Peierls instability, is also predicted to hold for TGB phases [11] and should produce algebraic decay of the scattering along the directions Q_y and Q_z rather than true Bragg singularities. This is however a small effect, basically invisible at our experimental resolution. In spite of the complex profile of the scattering, which is broad with different widths along the three directions of reciprocal space, in the remainder of the paper, we will refer to the diffracted features as Bragg peaks (instead of quasi-Bragg or Bragg-like peaks) for the sake of simplicity.

3 Results and discussion

Samples of uniform thickness (25 μm) were studied first. Diffraction patterns were recorded in the TGB_C phase at 102.6 °C where the helical pitch is of order 2.0 μm [9]. The glass cells were mounted at the appropriate Bragg incidence angle as described previously and vertically scanned along the z-axis in 40 μm steps. We checked the stability of the liquid crystal in the intense focused beam and found that the diffraction patterns changed for exposures longer than 0.4 s towards a diffuse (cholesteric like) diffraction ring. We chose to limit exposure times to 0.13 s, hence limiting the signal to noise ratio of the recorded images. Figure 4 shows such an image. The diffraction pattern clearly exhibits the expected set of Bragg spots, hence revealing a commensurate lockin twist angle $\Delta = 2\pi/18$. The detected spots are clearly broader than the instrumental resolution. The X-ray beam incidence was chosen in such a way that four Bragg rods of the reciprocal space intersected the Ewald's sphere: the envelope then exhibits four maxima of intensity as explained above. Moreover we can observe that the diffraction ring is partially doubled.

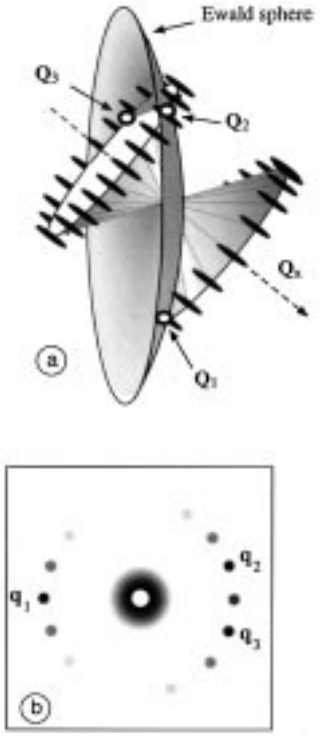

Fig. 3. Bragg diffraction from a well aligned TGB_C sample. (a) Scattering geometry showing the intersection of the Ewald sphere with the TGB_C reciprocal lattice (open circles). The orientation of the sample is chosen in such a way that wavevector $\mathbf{Q}_1$ on one ring is set exactly at Bragg incidence. The Ewald sphere then intersects the other ring at two symmetrical wavevectors $\mathbf{Q}_2$ and $\mathbf{Q}_3$. (b) Sketch of the expected diffraction pattern, considering the finite extension of the Bragg spots along the helical axis Q_x. The Bragg intensity appears as if distributed on a ring of radius Q_0. It exhibits maxima at positions $\mathbf{Q}_1$, $\mathbf{Q}_2$ and $\mathbf{Q}_3$ and falls off rapidly upon moving away from these three Bragg positions. Note that the angular width of the region where Bragg scattering is detected is larger on the $\mathbf{Q}_2$, $\mathbf{Q}_3$ side.

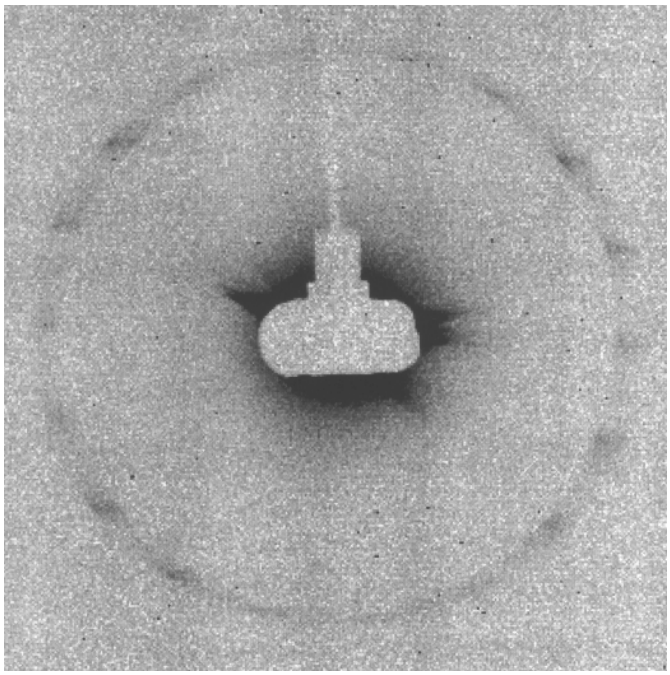

Fig. 4. Diffraction pattern recorded in a cell of uniform thickness $D = 25$ μm at $T = 102.6\,^{\circ}$C in the TGB_C phase. Exposure time is 0.13 s, beam size at sample position is 20×40 μm^2. The number of helical pitches is about 12. Note the four positions of scattering maxima: two on the left arc of the ring and two on the right arc of the ring, respectively. Similar commensurate-like patterns with 18- fold symmetry were observed everywhere throughout the sample (more than 300 different places). No effect of p/q-mosaicity was observed at this scale.

This was due to some structure of the incident beam and was not observed in subsequent experiments. The diffraction ring shift due to the intersection of the Ewald sphere with different parts of the Bragg rods is of the order of $\delta Q/Q = 1.5 \times 10^{-2}$ and completely negligible within our experimental resolution.

The important result is that all recorded images were similar (*i.e.* were indicative of a commensurate structure) throughout the sample. We investigated more than 300 different places. A few indistinct images lacking the 18-fold symmetry, were observed and shown to be associated with local defects (dust particles or small gas bubbles). We conclude that any hypothesis claiming spatial variation of the local value of the commensurability ratio α has to be ruled out for spatial variations over length scales larger than probed by the experiment; namely, 20×40 μm^2. Nevertheless, the number of helical pitches across the sample is not large ($= 20$). The effect of finite thickness and surface anchoring cannot be neglected.

In order to investigate the effect of thickness on commensurability, wedge samples were studied in a second experiment. The signal to noise ratio was improved *via* a numerical superposition of images. We checked that successive images (0.13 s exposure) recorded at 60 s intervals (same position) were identical (*i.e.* no effect of the irradiation was detected). By synchronising the image accumulation on the CCD camera with the operation of a fast shutter and by implementing, in software, automatic image summation, we obtained for each position an image with reasonably low noise. These images were produced by the summation of 5 to 20 individual images (0.13 s single exposures and 60 s waiting time between successive exposures). Several series of about 80 images were recorded while translating the wedge cell, with 40 μm steps, in the direction of increasing thickness. The typical diffraction patterns are shown in Figure 5 for five different positions along the wedge, *i.e.* different cell thicknesses. Note that the diffracted intensity exhibits the three typical maxima ($\mathbf{Q}_1$ on one branch, $\mathbf{Q}_2$ and $\mathbf{Q}_3$ on the other side) sketched on Figure 3b, hence confirming that the orientation of the helical axis is define to better than the Bragg angle (0.7 degrees).

To analyse the data, we first integrated the scattered intensity over the whole diffraction ring and plotted the resultant integrated intensity *versus* thickness D (Fig. 6). D is always much shorter than the absorption length which is in the mm range. The integrated intensity scales linearly with thickness (*i.e.* with scattering volume) as it should up to 23 μm and then deviates towards lower values. This result implies that the quality of the alignment is constant for thicknesses up to 23 μm but decreases for thicker samples until eventually, for thicknesses above 30 μm, defects can be observed optically.

Measurements were taken in the wedge cell at three different temperatures, 102.0, 102.2 and 102.6 °C, with nearly identical results. Figure 7 summarizes all the observations recorded at 102.2 °C. The angular position of all the Bragg spots corresponding to individual smectic slabs is plotted as a function of thickness (triangles) whereas the center of the broad spots only is given for larger thicknesses (squares). Three regions associated with the three different types of diffraction patterns of Figure 5 can be distinguished.

In the thin region (Zone 1, $D < 8$ μm), characteristic TGB diffraction patterns are observed with distinguishable bunches of Bragg spots. With increasing thickness, they appear in groups of 2, 3 (Fig. 5 - Zone 1) and 4 spots corresponding to regions with 2, 3 and 4 helical pitches respectively separated by Grandjean-Cano lines. The position of the first Grandjean-Cano lines ($D = 5$ and 8 μm *i.e.* 3 μm step) is larger than the value of the helical pitch measured in reference [9] (2.5 μm) at this temperature. The discrepancy is probably the result of the thin edge of the wedge being a region of strong elastic stress. It is worth noting that the diffraction patterns recorded in between two GC lines are exactly similar (about 10 images running over 400 μm) which shows that the whole region is a single crystal (no p/q-mosaicity). The thickness of each individual slab thus increases linearly with the wedge thickness, with no rotation of any slab about the helical axis. By counting the number of pitches (equal to the number of diffraction spots in each bunch) and the number of slab per pitch (equal to the number of bunches

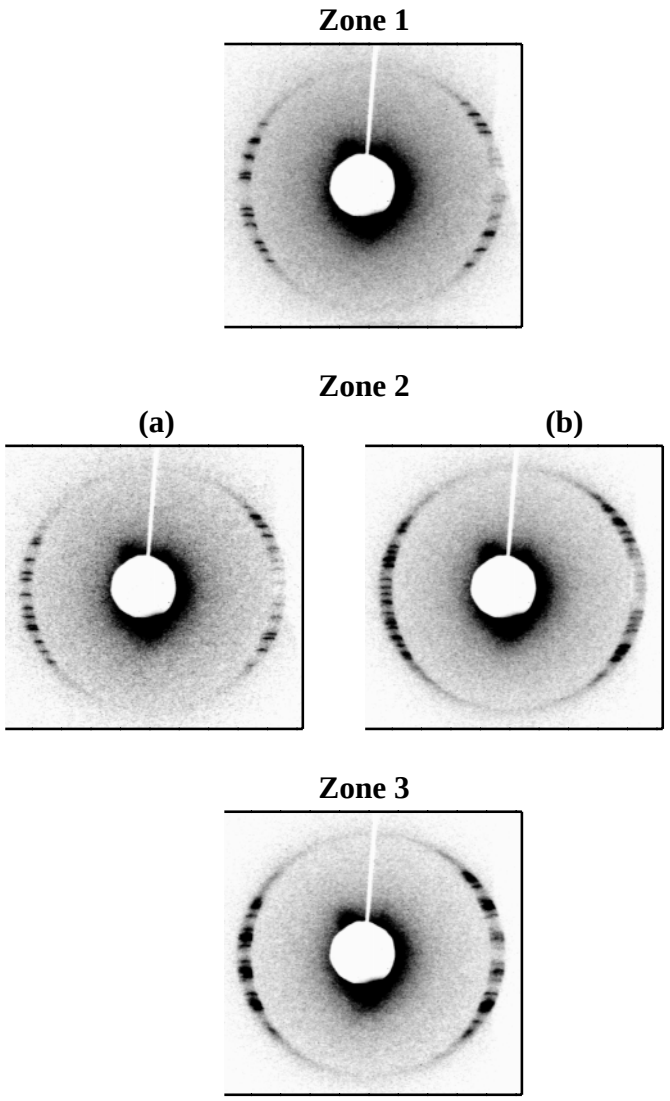

Fig. 5. Diffraction patterns recorded at four different thicknesses D in the TGB_C phase at $T = 102.2\,^{\circ}C$. Zone 1, $D = 7.5\ \mu m \approx 3$ pitches. Each recorded Bragg spot corresponds to one single smectic C slab. The rectangular shape, elongated along horizontal axis is due to the horizontal divergence of the focused X-ray beam. The distribution of Bragg spots in bunches of three (corresponding to pitch number 1, 2 and 3 successively) is clearly visible in the north-west quarter of the ring. This is a clear evidence of an incommensurate distribution of the smectic slabs. The twist angle Δ is about $2\pi/22 + 2.10^{-3}$ rd. Zone 2, (a) $D = 9\ \mu m \approx 4$ pitches. Individual Bragg spots are still visible but begin to fill evenly the ring. This is again the signature of an incommensurate distribution. (b) $D = 18\ \mu m \approx 9$ pitches. The ring is almost uniformly filled as for an incommensurate distribution. Zone 3, $D = 21.4\ \mu m \approx 11$ pitches. The too numerous individual Bragg spots cannot be distinguished any more. However, their angular distribution around the ring of scattering is no longer uniform: an 20-fold modulation of the intensity clearly shows up. The angular spread of the new broad spots is about 12 degrees.

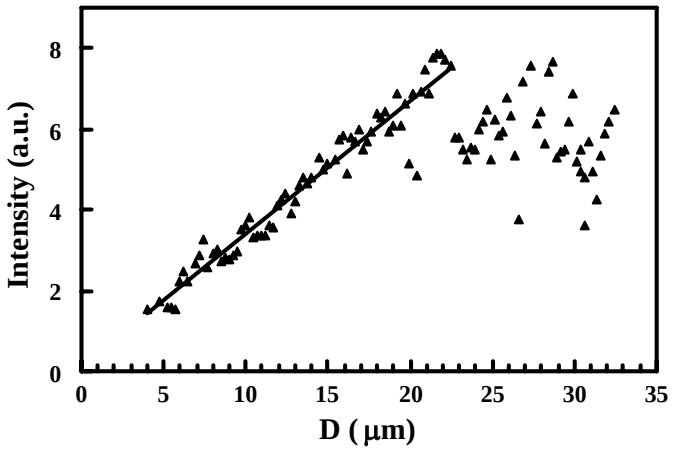

Fig. 6. Plot of the total scattered intensity, integrated over the Bragg ring, *vs.* thickness. Linearity shows that the quality of the alignment is good up to 23 μm. Partial disorientation of the TGB_C phase occurs for higher thicknesses.

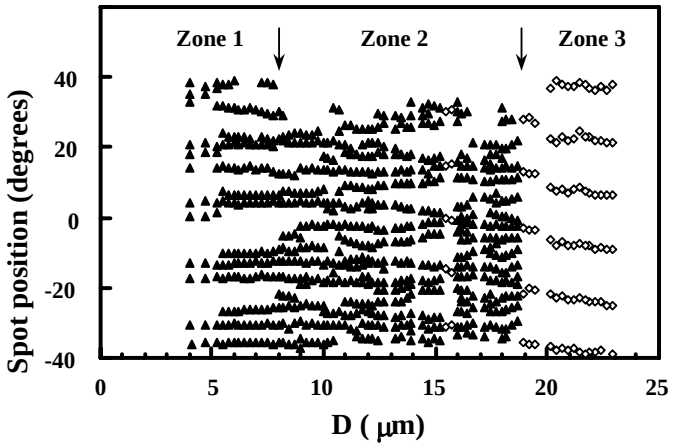

Fig. 7. Plot of the angular position of the observed spots *vs.* thickness. Triangles denote individual Bragg spots diffracted by single smectic slabs whereas diamonds correspond to the center of the broad maxima of diffraction. Note that the position of the single Bragg spots is fairly stable between adjacent GC lines, which shows that the thickness of the smectic slabs increases at constant twist angle with increasing sample thickness D.

on the diffraction ring), the slab thickness between two GC lines varies from 75 to 120 nm.

The non superposition of Bragg spots diffracted from pitch n and $n + 1$ (about 4 degrees or 7×10^{-2} radian between 2 spots in the same bunch) is the signature of an incommensurate TGB structure. We can characterise the incommensurability by incorporating a constant, ε

in the expression for the twist angle; namely $\Delta = 2\pi[(p+\varepsilon)/q]$. In the thin region, the twist angles, which result in the observed diffraction features, have the average value $\Delta = 2\pi[(1+0.011)/22]$. Moreover, due to the limited number of distinct spots in this region, it is reasonably possible to identify Bragg spots diffracted by adjacent slabs, hence providing a direct local measure of the twist angle Δ at different depths in the sample. We found that this value is not constant: Δ exhibits small local deviations from its average value (typically $\pm 7\%$) which means that the grain boundaries are not exactly identical.

In the intermediate region (Zone 2, 8 μm $< D <$ 18.8 μm) we measure an almost isotropic (*i.e.* without any regularity) Bragg spot distributions. Figures 5a and 5b show the diffraction patterns obtained at 9 μm and 18 μm, respectively. Bragg spots are very peaked with the number of individual Bragg spots increasing with the thickness. This particular diffraction pattern is observed for the first time and reveals an incommensurate TGB_C structure.

Finally, in the thicker region of the cell (Zone 3, 18 μm $< D <$ 30 μm) individual Bragg spots are nolonger distinguishable: most of them merge instead into a small number of equispaced broad spots (Fig. 5 - Zone 3) hence revealing a q-fold modulation of the intensity of the ring of scattering. It is evident that the broad spots are a composite structure of unresolved resolution-limited peaks. The angular width of the broad spots is the envelope of these individual peaks.

Interestingly, the wedge experiments demonstrate that q-fold modulation shows up only at a sufficiently large sample thickness. Thin samples ($D < 18$ μm) for which surface effects are expected to be strong, clearly exhibit an incommensurate angular distribution of the smectic slabs.

Another important result of the present experiments is the demonstration that the diffraction patterns observed previously from 1×1 mm^2 areas, typical for conventional rotating anode measurements [6,7], do not result from a mosaic distribution of smaller crystallites with possibly different values of α. The angular distribution of the smectic slabs probed at the microfocus spatial resolution (20×40 μm^2) is uniform over 1×1 mm^2 patches. An interesting consequence is that rotating anode experiments performed on samples of constant thickness give the same relevant information about commensurability as the microfocus beam (this is not true for wedges where a large beam gives an average signal over a wide range of thicknesses). Consequently, since similar q-fold distributions were observed in all samples at all temperatures in all experiments with TGB_C phases [6,7], the possibility that it is a fortuitous effect of p/q-mosaicity has to be ruled out.

The broad width of the Bragg spots recorded in the thickest regions ($D > 18.8$ μm) can be experimentally interpreted in either one of two ways:

(i) The twist is commensurate on average *i.e.* the individual Bragg spots occur in a statistical distribution of angles q around the TGB_C ring with a q-fold modulated probability $P(q)$. For instance, a probability

$$P(q) = \frac{1}{q\sigma_\theta\sqrt{2\pi}} \sum_{i=1}^{q} \exp[-(\theta - 2\pi i/q)^2/2\sigma_\theta^2] \qquad (1)$$

would produce q equispaced Bragg spots of width σ_θ (provided $\sigma_\theta < 2\pi/q$). In this case, the modulation should show up at all temperatures, the quality of the statistics should improve with thickness but the width σ_θ is independent of thickness.

(ii) The twist angle Δ is incommensurate (*i.e.* $\Delta = 2\pi(p+\varepsilon)/q$ with $\varepsilon \ll p/q$). Individual Bragg peaks gather in broader spots of width $2\pi\varepsilon(n-1)/p$ for a sample of thickness n pitches. The scattering pattern exhibits a q-fold symmetry as long as the width of the spots $2\pi\varepsilon(n-1)/p$ is significantly lower than their separation $2\pi/q$ [*i.e.* $(n-1)\varepsilon < p/q$]. In this case, the q-fold modulation is a finite size artefact, its amplitude should depend dramatically on temperature (*via* Δ) and the width of the spots should increase as n.

The most convincing way to discriminate between case (i) (true commensurability) and (ii) (finite size effect) would be to analyze the width of the recorded Bragg spots as a function of thickness. The observed width σ_θ is indeed constant, but the experimental range of available thicknesses (from 18 to 23 μm) is too narrow to warrant a definitive conclusion. One way to extend the range of sample thicknesses probed is to change the temperature of the sample. Since the TGB_C pitch is temperature dependent, the number of pitches for a fixed sample thickness can be increased by changing the temperature. This then is effectively equivalent to increasing the cell thickness. Unfortunately, whether we change the actual or effective cell thickness, the situation is still complicated by the constraints imposed by using planar-anchoring surface treatments to freeze the sample orientation at both bounding interfaces. An elegant solution to avoid this twist constraint, which we intend to pursue in the future, would be to study the temperature dependence of the TGB_C diffraction pattern for a sample with one free surface.

4 Conclusion

Investigation of the helical TGB_C structure with a microfocus X-ray beam has provided invaluable information about the angular lockin that may or may not lead to a q-fold commensurate structure.

First of all, probing the sample with a spatial resolution of 20×40 μm^2, over 10^3 finer spatial resolution than possible in conventional rotating anode experiments, has definitely ruled out the possible problem of observations being biased by a polycrystalline mosaic. Not only are the microfocus diffraction patterns the same at any place throughout samples of uniform thickness, but also experiments in wedge cells with strong planar anchoring have shown that single TGB_C crystals (*i.e.* with uniform orientation of all individual smectic slabs) extend all the way in between adjacent Grandjean-Cano steps. Changes

in cell thickness are accommodated *via* correlated changes in the smectic slab thickness.

Second, the study of wedges has demonstrated that the q-fold symmetry, which constitutes the so-called commensurate arrangement of the TGB_C, results from a statistical angular distribution of a large number of slabs. Thin regions (2 to 4 pitches) reveal the absence of exact commensurate lockin and some scatter in the twist angle of the grain boundaries. In thicker regions, the superposition of a large number of Bragg spots builds up the angular distribution function which turns out to exhibit the q-fold commensurate modulation. The independence of the Bragg spot angular width on the number of pitches provides evidence against the possibility that the width is due to a small incommensurability.

Third, the present microfocus experiments validate previous systematic observations of q-fold symmetry in TGB_C phases with a large tilt angle [6,7]. Altogether, these results show that the q-fold symmetry is not fortuitous and can be considered as clearly experimentally established. Its origin (anchoring effect or intrinsic interaction) is however still unknown. Theoretical efforts are certainly needed regarding this point.

Finally, the present work gives some insight into the application of an intense focused X-ray beam to probe fragile complex fluid materials like liquid crystals. Sample degradation does occur and limits the quality of the data. The main undesirable effect seems to be a local heating of the irradiated area that melts the liquid crystal into a higher temperature phase. We showed that this problem can be solved by using a series of short X-ray pulses and summing up the data from several pulses in order to improve the signal to noise ratio if necessary. An interesting application could be the study of a slow dynamics of a first order liquid crystal phase transition.

References

1. P.G. de Gennes, Solid St. Commun. **10**, 753 (1972).
2. S.R. Renn, T.C. Lubensky, Phys. Rev. A **38**, 2132 (1988).
3. S.R. Renn, T.C. Lubensky, Mol. Cryst. Liq. Cryst. **209**, 349 (1991); S.R. Renn, Phys. Rev. A **45**, 953 (1992).
4. J.W. Goodby, M.A. Waugh, S.M. Stein, E. Chin, R. Pindak, J.S. Patel, Nature (London) **337**, 449 (1989).
5. H.T. Nguyen, A. Bouchta, L. Navailles, P. Barois, N. Isaert, R.J. Twieg, A. Maaroufi, C. Destrade, J. Phys. II France **2**, 1889 (1992).
6. L. Navailles, P. Barois, H.T. Nguyen, Phys. Rev. Lett. **71**, 545 (1993).
7. L. Navailles, H.T. Nguyen, P. Barois, N. Isaert, P. Delord, Liq. Cryst. **20** 653 (1996).
8. Y. Galerne, Phys. Rev. Lett. **72**, 1299 (1994).
9. N. Isaert, L. Navailles, P. Barois, H.T. Nguyen, J. Phys. II France **4**, 1501 (1994).
10. L. Navailles, R. Pindak, P. Barois, H.T. Nguyen, Phys. Rev. Lett. **74**, 5224 (1995).
11. J. Toner, Phys. Rev. B **42**, 8289 (1991).